Vol. 15 • No. 21 • May 24 • 2019

www.small-journal.com

NANO · MICRO small

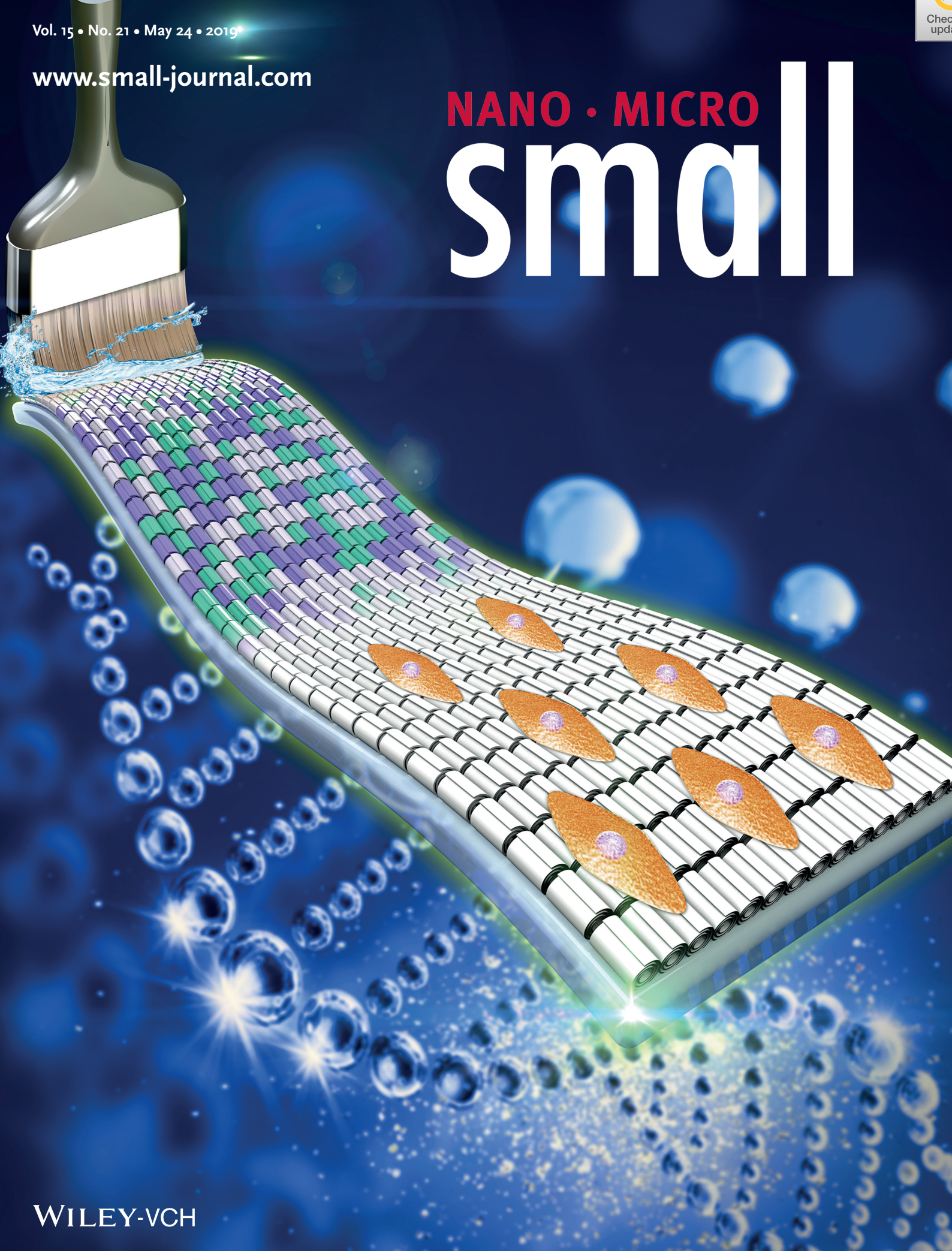

WILEY-VCH

NANO · MICRO small
www.small-journal.com

Clay Nanotubes Aligned with Shear Forces for Mesenchymal Stem Cell Patterning

Xiujuan Zhao, Changren Zhou, Yuri Lvov, and Mingxian Liu**

Aligned halloysite nanotubes on solid substrates are fabricated by a shearing method with brush assistance. These clay nanotubes are aligned by shear force in strip-like patterns accomplished with drying ordering at elevated temperatures. The nanotubes' orientation is governed by "coffee-ring" formation mechanisms depending on the dispersion concentration, nanotube charge, and speed of thermos-evaporation. Polarized light irradiated through the patterns demonstrates birefringence and confirms the orientation. Scanning electron microscopy and atomic force microscopy show that the nanotubes are aligned along the direction of the wetting lines above 4 wt%, while they are not oriented at lower concentrations. Halloysite concentration, drying temperature, and type of brush fibers affect the pattern ordering. The aligned halloysite systems on glass, tissue culture plates, and polymer films, provide a promising platform for biocell guiding. Human foreskin fibroblasts proliferated well on the aligned clay patterns and the cell orientation agrees with the nanotube direction. Human bone mesenchymal stem cells (HBMSCs) are also cultured on the organized halloysite coating. The clay patterns support HBMSC proliferation with alignment, and such nanostructured substrates promote osteogenesis differentiation without growth factors. This facile method for preparing aligned halloysite patterns on solid substrates is very promising for surface modification in biotissue engineering.

1. Introduction

Engineered tissue scaffolds provide mechanical and geometric supports for the biocell growth and patterning. The scaffolds mimicking, design of the structures of extracellular matrix within natural tissue on the surfaces of cell–adhesive substrates is important. The tissues such as nerves, bones, skin, and muscles exhibit anisotropic architecture necessary for retaining their physiological functions.[1–4] An aligned fibrous structure of skeletal muscle, tendon, and directed tissues allows for enhanced supporting movements and mechanical load.[5,6] Various types of scaffolds that have an oriented structure for cell aligning with promoted functions have been developed,[7,8] including electrospun nano-/microfibers, 3D printed tissues, and anisotropic porous scaffolds with freezing-drying technology. These studies demonstrated that the cells response to the physicochemical cues of the culture substrates activating relevant receptors, which results in the specific cellular morphology, migration, proliferation, and differentiation.[9,10] However, these fabrication methods for ordered structures are difficult in applications, i.e., electrospinning is not efficient for volume environment for cells. 3D printings lack of fine structure at nanoscale due to the limited working precision. The uncontrollable ice crystal growth in freeze-drying methods leads to nonuniform pore structure.

Recently, elongated nanoparticles with high aspect ratio have attracted special interest as the building blocks for biomedical materials because of their mechanical, electrical, and magnetic properties.[11] Nanotubes with hollow structure are especially attractive, due to the possibility of functionalization their end and inner/outer walls for controlled loading drugs, DNA, and proteins. Although, only carbon nanotubes were used for this purpose, which is limited by low biocompatibility and the carcinogenic nature of this material. For example, their cell penetration initiated cancer and injection to the lungs of mice with carbon nanotubes caused asbestos-like pathogenicity.[12] We suggest development of organized tissue scaffold based on biocompatible halloysite clay nanotubes that we introduced for material research.[13–16]

Halloysite nanotubes (HNTs) are natural nanotubes with external diameters of 50–70 nm, internal lumen of 10–15 nm and $Al_2Si_2O_5(OH)_4 \cdot nH_2O$ formula.[17,18] One of the unique features of these nanotubes is different inside/outside chemistry (Al_2O_3 and SiO_2) allowing for their selective modification. Due to biocompatibility and very low toxicity, halloysite are the

Dr. X. Zhao, Prof. C. Zhou, Prof. M. Liu
Department of Materials Science and Engineering
Jinan University
Guangzhou, Guangdong 510632, P. R. China
E-mail: liumx@jnu.edu.cn
Prof. Y. Lvov, Prof. M. Liu
Institute for Micromanufacturing
Louisiana Tech University
Ruston, LA 71272, USA
E-mail: ylvov@latech.edu
Prof. Y. Lvov
Department of Theoretical Physics and Quantum Technologies
National University of Science and Technology "MISiS"
Moscow 119049, Russia
The ORCID identification number(s) for the author(s) of this article can be found under https://doi.org/10.1002/smll.201900357.

DOI: 10.1002/smll.201900357

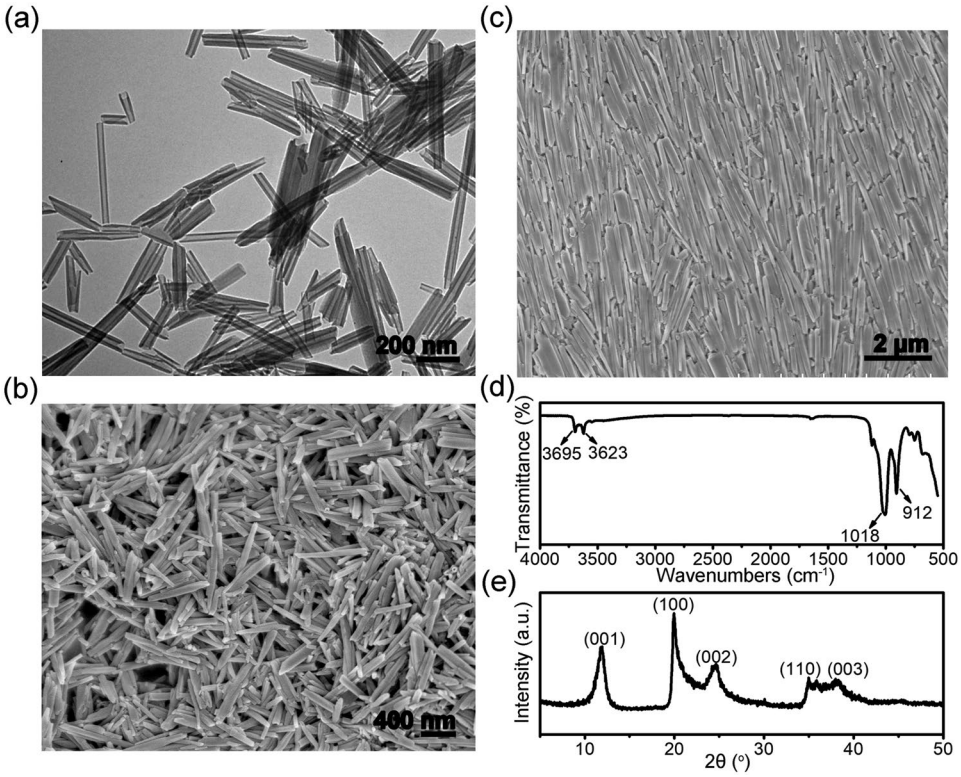

Figure 1. Halloysite images: a) TEM, b,c) SEM (b – random and c – oriented nanotubes with better droplet-edge ordering), and d,e) FTIR spectra and XRD patterns.

perspective nanomaterial for biomedical applications and were already utilized in cosmetics and animal care.[19–21] Superb nanosafety of the halloysite was demonstrated on different cell cultures, infusoria, microworms, zebrafish, and mice (halloysite is safest among clays, such as kaolin, bentonite, montmorillonite, and silica).[17] These clay nanotubes have advantages such as low cost, much availability, and easy modification based on silane chemistry.

Elongated nanotubes are most efficient for the assembly into the anisotropic patterns.[18] The oriented architectures of carbon nanotubes guide cell orientation at an efficient rate, although the biocompatibility of these materials is low which leads to poor cell proliferation.[8,11,19–21] The driving forces for nanotube ordered patterns include electrical field,[22] shear, and magnetic forces.[23] More recently, the anisotropic patterns of nanotubes were made via capillary force induced self-assembly. We found that clay nanotubes can be aligned along the edge of a drying droplet of halloysite suspension associated with phenomenon known as "coffee rings" explained by the Onsager's theory for ordering of highly charged nanorods (**Figure 1**c). During this thermoaccelerated drying, three-phase contact line between air, suspension, and the solid substrate is fixed, and evaporation pulls liquid from the droplet center thus pushing the suspended nanotubes toward the edges. The accumulation of tubes at the circumference increases their concentration up until a certain level when electrostatic interaction produces oriented arrays of nanotubes (in our case – halloysite). However, this method cannot make large-scale oriented structures of halloysite due to the limitation in narrow circles (the edge vicinity).

A simple shearing/drying deposition using brushes to prepare periodic zigzag structure of DNA was recently suggested.[24] The resultant patterns were employed as a template to control the alignment of liquid crystals. We produced aligned HNTs patterns guided by shear forces provided by brushes and further controlled by thermoevaporation. Additionally, we induced multiple wet lines of preoriented halloysite dispersion followed with drying alignment. This method is versatile, simple and does not need complicated instruments. Moreover, large-scale oriented halloysite patterned surface can be prepared both on hard and soft substrates. The influence of brush types (fiber diameter, bristles softness, and periodicity), halloysite concentration, and drying temperature were optimized for the best hierarchical pattern architectures. The orientation degree of nanotubes and 3D topology of the patterns formed at different concentration were examined.

Human foreskin fibroblasts (HFFs) and mesenchymal stem cells (HBMSCs) were then cultured on the halloysite patterns and their proliferation and orientation behavior were evaluated. We found influence of the nanotubes orientation on osteogenesis differentiation of HBMSCs. This strategy was further used to modify polylactide based scaffolds and chitosan membrane with aligned clay nanotubes for directed cell growth. This simple alignment method of clay nanotubes is very perspective for biomaterial surfaces modification to regulate cell behaviors and functions.

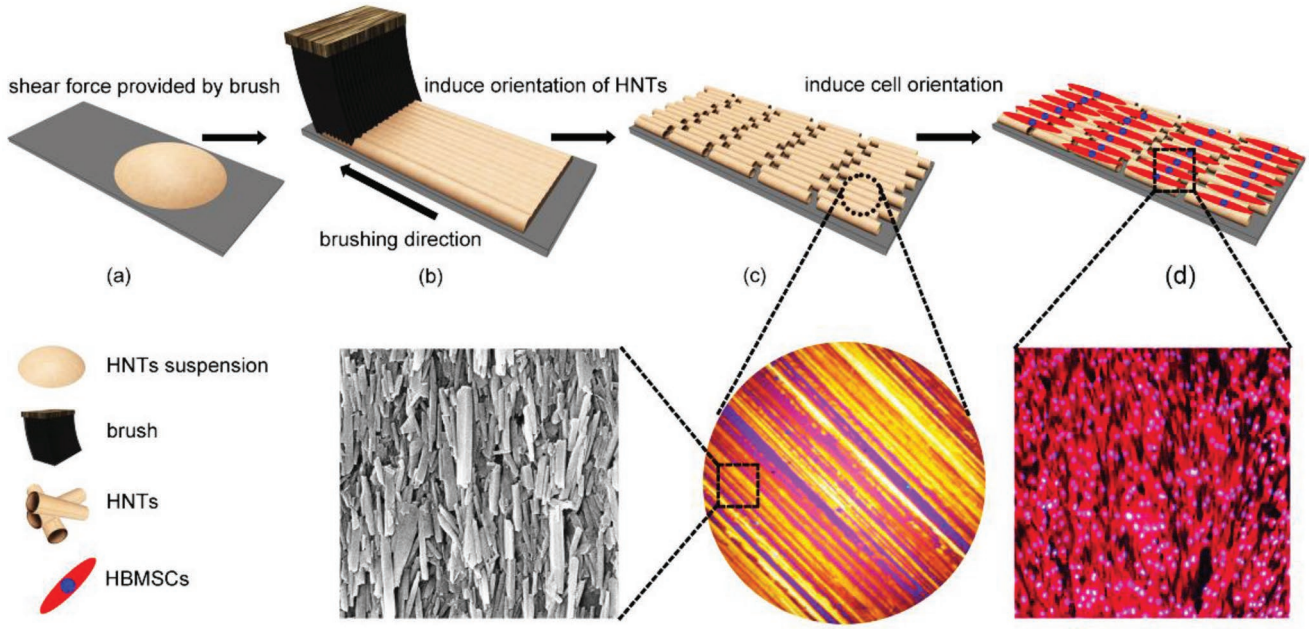

Figure 2. Schematic illustration of preparing the ordered HNT-arrays and guiding the cell orientation.

2. Result and Discussion

2.1. Characterization of HNTs

Figure 1 shows the scanning electron microscopy (SEM), TEM images, Fourier transform infrared (FTIR) spectrum, and X-ray diffractometer (XRD) pattern of halloysite. The length range of the nanotubes is between 400 and 600 nm. From the TEM images, the tubular structure with empty lumen is presented (outer diameter is 50–70 nm and inner lumen of 10–15 nm width). These nanotubes are well charged in water with zeta-potential of ≈−35 mV due to the special purification procedure (see the Experimental Section). FTIR spectrum shows typical absorption peaks at 912 cm^{-1} (O—H deformation of inner hydroxyl groups), 1018 cm^{-1} (Si—O stretching peak of silica group), 3623 cm^{-1} (O—H inner hydroxyl groups), and 3695 cm^{-1} (O—H innersurface hydroxyl groups).[25,26] Raw clay nanotubes show characteristic X-ray (001) diffraction peak at $2\theta = 12.0°$ corresponding to the basal spacing of 0.73 ± 0.2 nm. The Bragg peaks at $2\theta = 20.0°$ and 24.8° were assigned to (020, 110) and (020) crystallographic planes.[15,27–29]

These nanotubes were used for production of ordered oriented patterns, as described in the Experimental Section and summarized also in **Figure 2**. Typically, we wetted the brush into 2–20 wt% of aqueous halloysite dispersion and applied it at a speed of 0.1 m s^{-1} to a solid support followed with drying at 40–80 °C using the thermostation. Such nanotube patterns were used for biocell adsorption and proliferation studies.

2.2. Optimization of Oriented Halloysite Architectures at Different Concentrations

The oriented halloysite arrays were studied with polarized light microscopy with the first-order retardation plate. Different colors of lines are observed as the sample rotate from 0° to 180° (**Figure 3**). When the nanotubes have random directions, the colors do not change in the polarized microscopy during rotation. When the oriented sample rotate at 45° or 135° between the cross polarizers, the brightest lines are observed indicating anisotropy with majority of the nanotubes oriented. When the orientation pattern is rotated for 360°, the images can be recovered as shown in the images in Figure S1 of the Supporting Information. This was also confirmed by SEM images presented further in Figure 5. These strip-like patterns remind DNA array orientation along the shearing visualized with polarized microscopy.[24]

Our halloysite architectures generated the birefringent effect attributed to the parallel array of the nanotubes. While the linear polarization light passes through the HNT-pattern, the X-light component is parallel to the optical axis and y is perpendicular to it, as depicted in the Experimental Section (Figure 9). When the x and y light components are skewed to the direction of P2 polarizer, they are decomposed but the light parallel to the P2 polarizer is visible.

The light appearance in Figure 3 varies from transparency to opaque, suggesting that the coating thickness increases with the concentration. Difference in thickness and refractive index for components of white light allow visibility of colorful pictures produced depending on the perfection of orientation. The birefringent effect defining the orientation was not found while we used 2 wt% and less concentration of the clay nanotubes. As the concentration increased, the lines became denser and colors become brighter shifting toward the yellow spectra side. The width and distance of stripe is then calculated (averaging 50 strips). The stripes become wider and the distance between neighbor strips was narrower with higher halloysite concentration.

When the halloysite dispersion concentration is low, the contact probability between the nanotubes and nylon bristle is reduced and the shear forces dissipate. Besides, the concentration of 1 wt% was found to be the smallest when "coffee-ring"

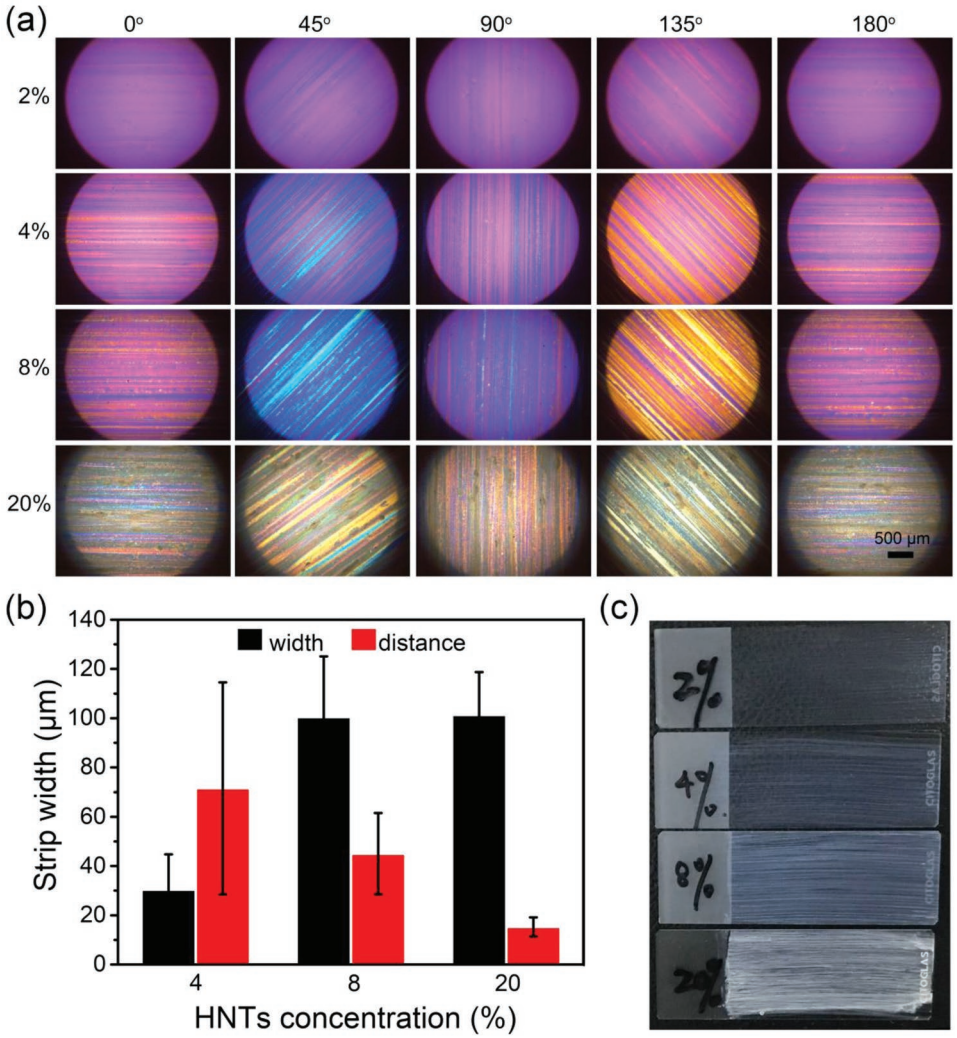

Figure 3. a) Polarized light microscopy images, b) stripe width, and c) appearance of HNT-coating formed with the different concentration using nylon brush (diameter: ≈120 μm; distribution density of bristles: 35 fibers mm^{-2}).

orientation mechanism was working for thermodrying ordering of clay nanotubes,[30] which is the main reason for lack of the tubes' orientation. With the increase of halloysite concentration above 2 wt%, it first has more efficient shear force during brush deposition, and second, synergistic switching-on the mechanism of Onsager's ordering of the charged nanotubes. The bright line becomes denser as the ordering of nanotubes increased. From Figure 3, we conclude that the best sample was prepared from the clay aqueous dispersion of 4 to 8 wt%. The intertube interaction which also may be characterized by dispersion viscosity affects the tube's alignment. Figure S2 of the Supporting Information shows that the dispersion viscosity becomes larger as the concentration increases.

2.3. Temperature, Brush, and Substrate Influence on the Tubes' Orientation

Halloysite concentration, brush type, substrate, and drying temperature affect the formed nanotube architecture. The elevated temperature accelerates the rate at which water evaporates during the drying of deposition of wet brush pattern. This enhances orientation of nanotubes due to electrostatic interaction. We used the thermos-station to heat the substrate during the halloysite brush coating. The nanotubes are randomly aligned if dried at 40 °C, but at 80 °C the strips show darker color (**Figure 4**), due to fast water evaporation. Thermal motion drives the nanotubes random after releasing the external force, but this is overweighted by Onsager electrostatic alignment at high concentration regions starting from the dispersion line edges.

Nylon, cosmetic, and tooth brushes provide different levels of orientation in the patterns. The cosmetic brush has the soft bristles, so the shear force provided by it is relatively weak. The space between the strips is large and the line color is bleak. It suggested that the nanotubes have no regular orientation. By contrast, the toothbrush has the hard bristles which provide more stress presenting bright strips and brighter colors.

The method of preparing oriented halloysite architecture was applied to modify the bioengineering scaffolds to mimic a structure of tissue. The bright optical fringes were found

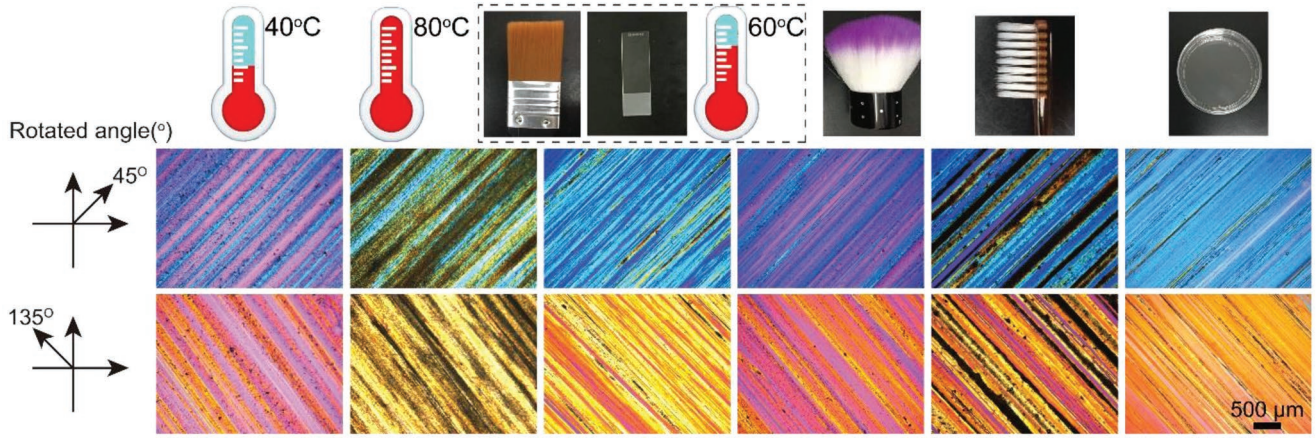

Figure 4. Polarized microscopy images of halloysite coating formed on glass at the different temperatures (three left pictures); and different brushes—cosmetic nylon and tooth brush (two right); the last image shows pattern on plastic dish (HNTs concentration: 8 wt%, w/v).

on the polymer culture dish or glass surfaces which proved clay nanotube organized arrays on both substrates (Figure 4). Figure S3 of the Supporting Information shows the polarized light microscopy images of oriented nanotubes with the different volumes of suspension that demonstrate a necessity of larger amount of halloysite in the single strip. Our nanotube architecture method is promising for preparing more complex hierarchical topographies, for example, using sequential brushing in parallel and perpendicular modes (Figure S4, Supporting Information).

2.4. Morphology of the Halloysite Patterns

As follows from polarized microscopy, nanotubes are randomly distributed at 2 wt% (and lower) concentration which also evident from SEM image in **Figure 5** while 4 wt% concentration sample gives well alignment along the brush wetting lines. The orientation degree of nanotubes at 4, 8, and 20 wt% concentrations was high, as characterized by their direction distribution with two characteristic peaks up and down, i.e., 90° and 270°. At 2 wt% there is no distinct orientation peaks in the plots demonstrating random halloysite orientation. The shear force provided by brush induces the best nanotube orientation at 4–8 wt%. Halloysite have the negative charges and its behavior is governed by electrostatic repulsive force between the tubes. The electrostatic repulsive force plays a key role on the colloid stability and charged nanotube alignment. The nanotube repelling remains weak until they reach the close packing corresponding to one nanotube in the 1 μm cube of water (corresponds to 4 wt% halloysite). Sufficient tube charge is needed to avoid the nanotube aggregation. When the HNT-concentration is low and the distance between the nanotubes is large, the repulsion is low and cannot provide alignment. However, the alignment occurs when the halloysite concentration is higher. According to the previous study, increasing concentration to 4–10 wt% gives stable halloysite dispersions.[31,32] Therefore, the colloidal stability followed with condensation of oriented nanotubes at higher temperature results in the coffee-ring phenomenon. Also, the dispersion viscosity is proportional to the concentration. Samples of 4 wt% HNT dispersion had optimal stability and viscosity resulting in good orientation.

The surface thickness and roughness of the oriented halloysite on substrates can be controlled by the suspension concentration. From the polarized microscopy images, the nanotubes are randomly distributed in the pink color areas. The other areas change its colors with the rotation angle and in these areas, nanotubes are oriented (Figure 3).

The nanotubes were aligned under the brush shear force at 4 to 20 wt% and the surface became rougher with the increase of concentration. At higher concentrations some convex protrusions can be found in the images. The controlled surface roughness is important for the interactions with biocells.[33–36] Aligned halloysite patterns were produced on the surface of one-layer polylactic acid printed scaffold and two-layer scaffold prepared by heat pressing (the same method is used to modify chitosan membrane scaffolds). Figure S5 of the Supporting Information shows good oriented structure of halloysite on the surface of these polymeric scaffolds. Our technique can be extended for coating ordered halloysite on other biomaterials, such as titanium alloy of orthopedic implant. Besides, halloysite can be converted into hydroxyapatite to further increase the osteogenic activity of this nanocomposite scaffold. Figure S6 of the Supporting Information shows atomic force microscopy (AFM) image and roughness of halloysite pattern formed at the different concentration. It also can be seen that the alignment of the tubes and increased roughness at high halloysite concentration.

2.5. 3D Profiles of Oriented Nanotube Architectures

The macroappearance of halloysite coating was observed by 3D scanning microscopy within 2.7 × 3.9 mm area (**Figure 6**), and difference between tops and valleys in the profile curves gave the pattern heights. The heights (pattern thickness) increased from 3.5, 4.1 to 33.5 μm with suspension concentration rise from 4, 8 to 20 wt%. It should be noted that the values in *y*-axis of height profiles are not the absolute value of height because the baseline is not from the bottom of the nanotube architecture. The thickness gradually becomes larger which agrees with the polarized microscopy

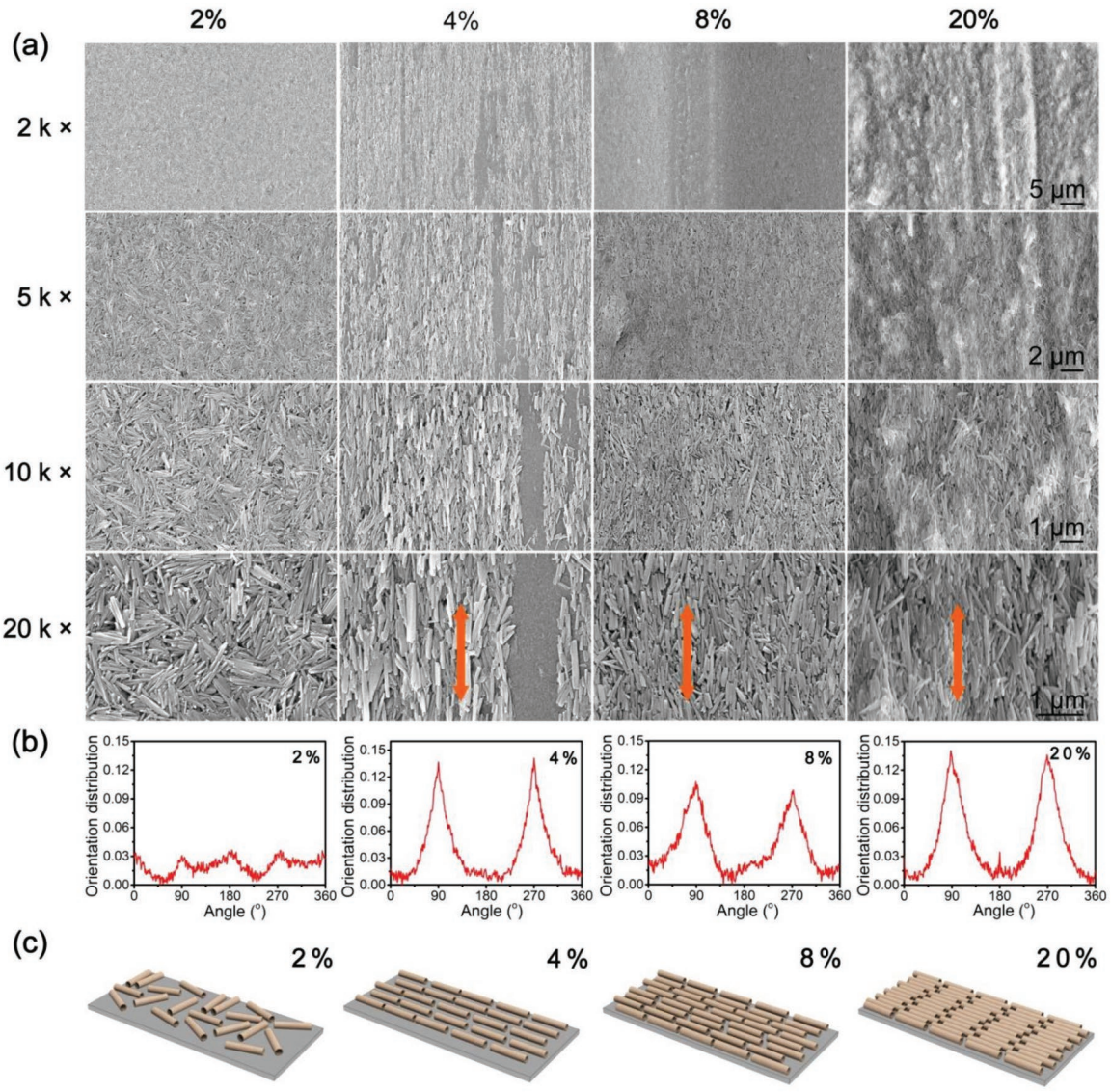

Figure 5. SEM images of halloysite coating formed at a) the different concentration, b) the orientation distributions, and c) the schematic illustration.

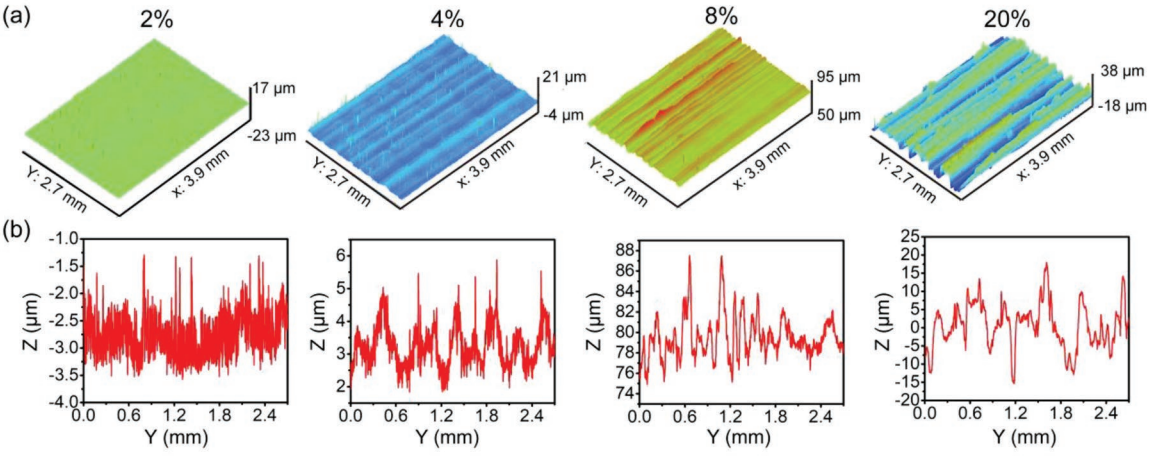

Figure 6. a) Topographic images and b) height profiles of HNT-coating formed at the different concentration.

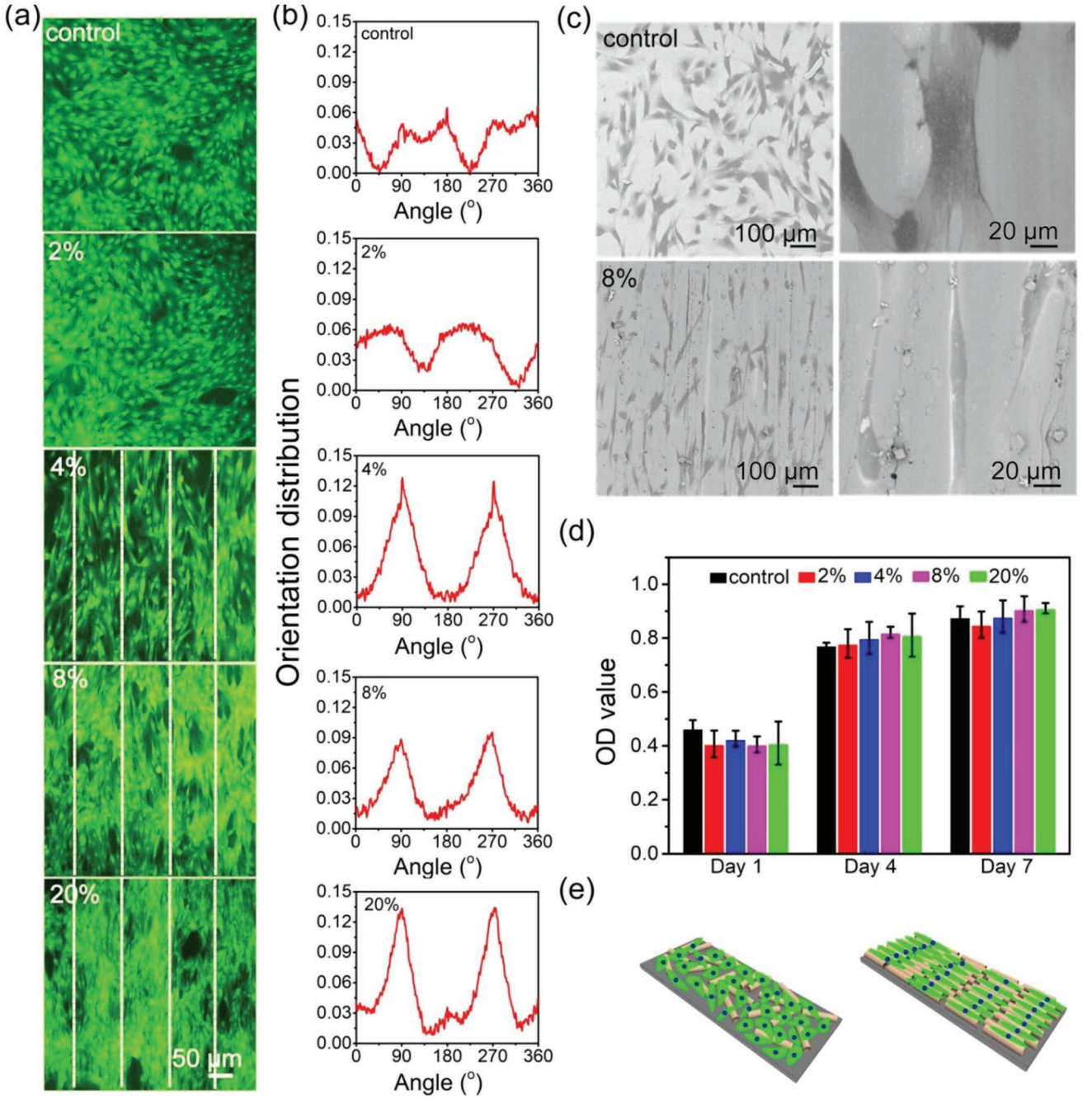

Figure 7. a) Fluorescence FITC staining of the cell patterns, b) orientation distribution, c) SEM image, and d) the cell proliferation, and e) schematic illustration for HFFs cultured on the aligned halloysite strip patterns.

colors becoming darker with increased concentrations. Some irregular grooves can be found at higher concentrations, probably related with overlapping of neighbor halloysite lines.

2.6. Fibroblast Alignment Induced by the Oriented Halloysite Patterns

Mimicking the native anisotropic structure of biological tissue in engineering scaffolds is crucial for advanced medicine. Some synthesized substrates were earlier designed for cell growth and alignment by the "contact guidance."[37–39] We prepared the oriented clay nanotube patterns to guide cell orientation. The morphology of human fibroblasts on the halloysite pattern was first observed with FITC staining (**Figure 7**a). The fibroblasts exhibited the polygonal morphology at the random HNT-coating, while they are elongated along the direction of the clay nanotube orientation at the ordered patterns (Figure 7). The directional angle distribution of the cells is consistent with the nanotube orientations

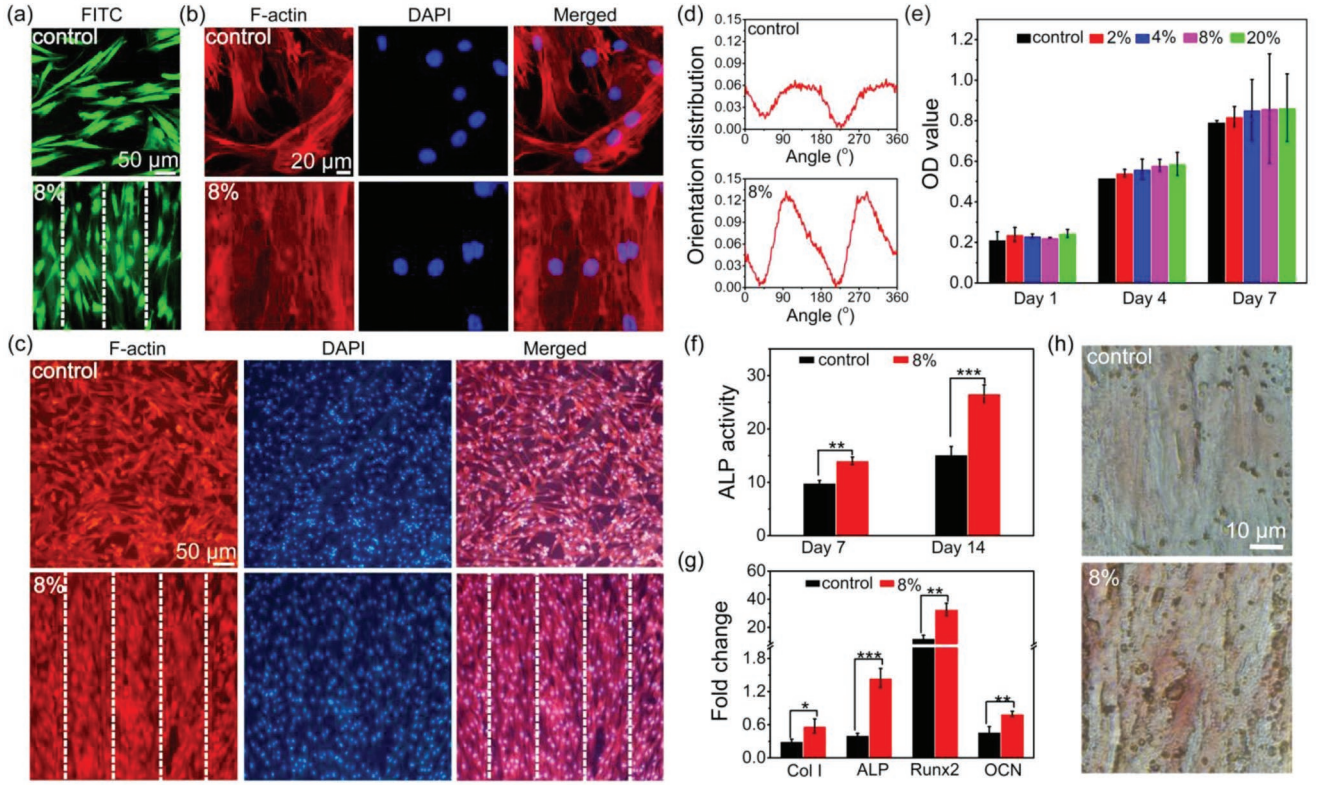

Figure 8. Fluorescent images of oriented and nonoriented (control) cells: a) HBMSCs – FITC cultured for 24 h, immunofluorescence staining of F-actin for HBMSCs cultured 3 d (b, × 40) and (c, × 10). d) Orientation angles distribution of the cells cultured for 3 d, e) their proliferation, and f) ALP activity after 7 and 14 d. g) The gene expression levels of Col I, ALP, Runx2, and OCN assessed by quantitative PCR after 14 d cultivation. Relative fold change in target gene expression is quantified by normalizing the target gene expression to GAPDH and h) ALP staining after cultivation for 7 d, (*$p < 0.05$, **$p < 0.01$, and ***$p < 0.001$).

obtained from SEM (no orientation was found for low 2 wt% halloysite patterns).

The characteristic peak at 90° and 270° (up and down orientations) of 4 to 20 wt% samples suggest that the cells are aligned uniaxially along direction of the nanotube orientation. From Figure 3c, the stripe width for 4 wt% pattern is about 30 μm and the distance between them is ≈70 μm. The cells preferred to grow along the areas of oriented halloysite. Figure 7c shows the cell morphology. Although, the direction of halloysite orientation cannot be observed at this magnification, the corresponding scratches by the brush have the same direction of the cells' orientation. Cell proliferation is evaluated by the CCK8 method after the cells were cultured for 1, 4, and 7 d. HFFs keep good proliferation with time (no difference in the cell viability with control group).

2.7. Mesenchymal Stem Cell Viability and Alignment on Oriented Halloysite Patterns

Regulating the stem cell functions is significant for design of tissue scaffolds. HBMSCs elongation has correlation with myogenic, osteogenic, and neural differentiation.[40–42] We evaluated behavior of HBMSCs cultivated on the oriented halloysite patterns. From the fluorescent images of FITC, F-actin, and DAPI staining, these stem cells display the elongated shape on the 8 wt% HNT-patterns while the control group had a random distribution. The cell orientation shows that the cells look in one up or down directions (90° and 270°).

HBMSCs were further studied with the laser confocal microscopy (due to the absorbance effect of the clay, we cannot completely exclude the nonspecific fluorescence). F-actin is a filamentous protein and can be observed with rhodamine labeling. At 8 wt% sample image, direction of cell microfilament is consisting with the one of halloysite strips. The SEM and polarized microscopy results proved the pattern strips having the same direction of halloysite tubes. From **Figure 8**, the numbers of HBMSCs have no difference for usual tissue culture plate and HNT-coated substrates.

Alkaline phosphatase (ALP) is an enhancer of the osteogenic activity. Its quantity was analyzed after HBMSCs cultivation for 7 and 14 d. The ALP activity onto oriented halloysite pattern was higher than in the control group, which suggests that the oriented nanoclay patterns promote osteogenic differentiation. The color of the best 8 wt% sample pattern is darker than the control group. Post-transcriptional regulation, translation, and post-translation regulation also play a role in the expression of the final protein.[43,44]

The gene expression levels after the cell cultured for 14 d was investigated for 8 wt% samples (Figure 8g); and the expression of Col 1, ALP, Runx-2, and OCN increased 2, 3.5, 2.7, and 1.7 times as compared to the control group. These results

proved that HBMSCs cultured on the oriented halloysite coating improved the cell differentiation. The elongated cell shape promotes greater differentiation because of its higher cytoskeleton tension (cell elongation played the important effect in directing HBMSCs osteogenic differentiation).[41,45] 1D HAp nanowires also can enhance the osteogenic differentiation of stem cells comparing with the nanorods.[20]

3. Conclusion

Oriented halloysite patterns were invented with brush shear force followed by the clay nanotube aggregation assembly. The halloysite concentration, charge, temperature, brush fiber type, and substrates influenced the formation of oriented architectural tubule ensembles. Spontaneously aligned nanotubes in the parallel strips demand for 4 to 20 wt% aqueous suspension concentrations and 60–70 °C for drying process. Shear force produced with 120 µm diameter nylon brash applied at speed 0.1 m s^{-1} gave the best results of oriented nanotube strips with maximal height of about 34 µm and periodicity of 30–100 µm providing templates for the organized stem cell arrays. SEM and AFM demonstrate that the clay nanotubes align along the shear force direction and the strip thickness becomes larger with the increased tubes' concentration. The nanoclay pattern may be prepared on glass slides, polymeric dishes, flexible films, and scaffolds.

Fibroblasts and HBMSCs had good proliferation and were aligned along the clay nanotube orientation. ALP quantitative analysis and staining proved that the oriented halloysite stripes promoted the differentiation of HBMSCs cultured for 7 and 14 d. The gene expression levels confirmed that the halloysite patterns improved osteogenic differentiation of the stem cells. This efficient method for fabricating the oriented clay nanotube arrays will be useful for producing biocell devices exploiting regular micro-/nanopatterns.

4. Experimental Section

Purification of HNTs: For better halloysite patterns, the commercial clay (Guangzhou Runwo Materials Technology Co., Ltd. China) was purified and impurities were removed by dispersion-centrifugation method. 2 wt% aqueous suspensions of halloysite were prepared and then kept for 24 h. The upper solution was centrifuged and freeze-dried. After repeating this cycle for three times, the purified halloysite were obtained, as characterized with SEM imaging and electrical zeta-potential of 35 mV.

Preparation of Aligned Nanotubes with by Different Brushes: 100.0 µL halloysite aqueous solutions with different concentration were spread onto the surface of glass slide substrates. The nanotubes were applied shear stress by different brush operated by hand and then the water evaporated rapidly at the temperature between 40 and 80 °C. The oriented halloysite architecture is shown in Figure 1. The halloysite concentration, brush types, substrates, and temperature on the process were investigated. The concentrations were 2, 4, 8 to 20 wt%). The brush fiber diameter and distribution density of bristles are presented in **Table 1**. The glass slides and the polystyrene culture dishes were used as the substrates. 40, 60, and 80 °C were found the best for thermodrying ordering of halloysite.

Characterization of HNTs: The morphology of halloysite was observed by SEM (Zeiss MERLIN FE-SEM, Germany) and TEM (Philips Tecnai 10, Netherlands). FTIR spectra of halloysite were collected on Bruker Vertex 70 spectrometer, where the powder samples were mixed with KBr and then pressed into thin IR-transparent disks. The crystal structure of halloysite was analyzed with an XRD (MiniFlex 600), Cu-Kα radiation. Data were collected over a 2θ range of 5°–50° with a scanning rate of 0.15° s^{-1}.

Table 1. Diameter and distribution density of bristles.

Brush type	Nylon brush	Cosmetic brush	Tooth brush
Diameter of bristles [µm]	120 ± 6	100 ± 5	205 ± 7
Distribution density of bristles [piece mm^{-2}]	35	60	9

Characterization of the Oriented HNTs Architecture: Steady shear viscosities of 2, 4, 8, and 20 wt% aqueous halloysite suspension, pH 6.5, were determined on a rotational rheometer (Discover) using a 25.0 mm diameter parallel-plate fixture. The morphology and the birefringence phenomenon of the oriented halloysite pattern were analyzed using a stereoscopic microscope with a polarized light component (ZEISS Stereo Discovery. V20, Germany). The microstructure of the pattern was also observed with SEM at 5 kV. The samples were sputtered with 1 nm gold prior the observation. The surface of halloysite pattern was also observed by the 3D surface topography analyzer (BMT EXPERT) and AFM (Veeco Instruments Inc). The halloysite pattern was labeled with fluorescein isothiocyanate (FITC, Shanghai Yeasen biotechnology Co., Ltd) and observed with fluorescence microscope.

Birefringent Characterization: The birefringent phenomenon of halloysite architectures was observed with the perpendicular polarized light. The angle between nanotubes' architectures and P1 polarizer is θ. The amplitude of linear polarization lights from the P1 polarizer is A. Thus, the projections of lights on the X-axis (fast-axis) and Y-axis (slow-axis) are $A\cos\theta$ and $A\sin\theta$ (**Figure 9**b). After passing though the halloysite pattern, the phase difference between the two components is δ[46]

$$\delta = \frac{2\pi}{\lambda}\left|n_x - n_y\right| d \tag{1}$$

where d is the thickness of crystal, n_x and n_y is the refractive index on the fast-axis and slow-axis. After the lights transmitting through the halloysite array, its component intensity is E_x and E_y

$$E_x = A\cos\theta, \quad E_y = A\sin\theta \cdot e^{i\delta} \tag{2}$$

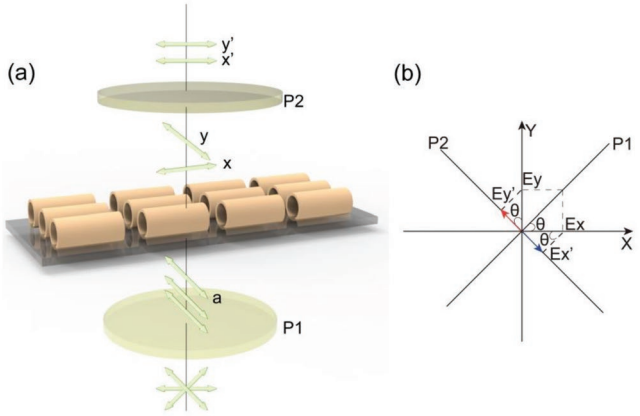

Figure 9. Illustration of birefringent generated by a) the nanotube pattern and b) components of lights transmitted through the polarizer and the pattern.

The components of E_x and E_y along the P2 transmission axis are as follows

$$E'_x = A\cos\theta\sin\theta, \quad E'_y = A\sin\theta\cos\theta \cdot e^{i\delta} \tag{3}$$

The two components having the same vibration direction and the phase difference are retained. They interference occurred and the light intensity is I

$$I = A^2\cos^2\theta\sin^2\theta + A^2\sin^2\theta\cos^2\theta - 2A^2\cos^2\theta\sin^2\theta\cos\delta \tag{4}$$

and after simplification

$$I = A^2\sin^2 2\theta\sin^2\frac{\delta}{2} \tag{5}$$

when the θ is 45° or 135°, light intensity has a maximum, which agrees with the observed results.

Cell Culturing and Seeding: For improving the stability of halloysite pattern during cell culture, the samples were soaked in 20 mL of 4.0% (v/v) 3-aminopropyl triethoxysilane in anhydrous ethanol solution for 2 min and then washed with ethanol.[47] The samples were then cut into 1 × 1 cm size. The halloysite pattern was sterilized in 75% (v/v) ethanol for 2 h, and washed for 10 min with PBS. After the halloysite coating was immersed into growth medium (90% DMEM, Gibco and 10% FBS, Gibco) for 12 h, HBMSCs (Cyagen Biosciences Inc) and HFFs (ATCC) were seeded on the coating at a density 2.0×10^4 cells cm^{-2} or 4.0×10^4 cells cm^{-2}. The culture medium was changed every 2 d.

Cell Morphology, Proliferation, and Differentiation: After the cells were cultured for a certain time, they were washed with PBS and fixed by 4% paraformaldehyde for 30 min, and permeabilized with 0.5% Triton-X100. Cell cytoskeleton was stained by FITC or rhodamine-labeled phalloidin probe for 1 h (TRITC Phalloidin, Beijing Solarbio Science and Technology Co., Ltd). The cell nuclei were stained with DAPI (Sigma) for 15 min. Finally, the samples were rinsed with PBS and studied with a fluorescence microscope (XDY-2, Guangzhou Yuexian optical instrument Co., Ltd., China) accomplished with a charge-coupled device. The cell morphology was also analyzed by SEM. A laser scanning confocal microscope (LSM 880) (Zeiss, Welwyn Garden City, UK) was used to visualize the immunofluorescence staining of F-actin (examined at 40 X magnifications).

The cell proliferation was evaluated using a Cell Counting Kit-8 (CCK-8) assay (BestBio). The OD value at 450 nm was measured after 1, 4, and 7 d of culturing. For evaluating the osteogenic differentiation ALP activity quantification was performed as in ref. [48] after the cell was cultured for 7 and 14 d. ALP was quantitized using the Alkaline Phosphatase Assay Kit (P0321, Beyotime, China), which was based on the conversion of colorless p-nitrophenyl phosphate (pNPP) to colored p-nitrophenol after coincubation for 15 min at 37 °C. The data were normalized to the total intracellular protein content measured with Protein Assay Kit (23225, Thermo scientific, USA). ALP activity was expressed in nanomoles of produced p-nitrophenol per min per milligram of protein. ALP staining was performed by using alkaline phosphatase color development kit (Nanjing jiancheng Bioengineering Institute, D001-2). After the cells were cultured for 14 d the levels of the mRNA for osteogenic specific genes (ALP, Runx2, OCN, and COL1) of HBMSCs were assessed using real-time PCR according to the previous method.[49]

Analysis of Orientation Degree: The orientation degree of nanotubes and the cell orientation induced by the substrate are analyzed by a 2D FFT image analysis method.[50–52] The 1024 × 768 px image of nanotubes taken by SEM was cropped to a square of 512 × 512 px. The 3072 × 2048 image of cells stained by FITC was analyzed and cropped 2048 × 2048 px to quantify the orientation degree of cells. By the 2D fast Fourier transform method, the SEM image and fluorescence image were converted into the frequency distribution. Pixel intensity was summed along the radius (from 0° to 360° with 1° increment) with the imageJ supported by an oval profile plug-in. All the dates were normalized and were plotted as a representation of frequency distribution.

All data are shown as means ± standard deviation (SD). Statistical analysis was carried out by a one-way analysis of variance, and $p < 0.05$ was considered as statistically significant.

Supporting Information

Supporting Information is available from the Wiley Online Library or from the author.

Acknowledgements

This work was supported by the grants from the National Natural Science Foundation of China (51473069 and 51502113), the Pearl River S&T Nova Program of Guangzhou (201610010026), and Key Laboratory of Biomedical Materials and Engineering of Ministry of Education, South China University of Technology. Y.L. acknowledges support of the Ministry of Education and Science of the Russian Federation in the framework of Increase Competitiveness Program of NUST (MISiS) K-2018-31, implemented by a decree from 16 March 2013.

Conflict of Interest

The authors declare no conflict of interest.

Keywords

alignment, halloysite nanotubes, shear force, tissue engineering

Received: January 18, 2019
Revised: March 15, 2019
Published online: April 8, 2019

[1] S. Jana, S. K. L. Levengood, M. Q. Zhang, *Adv. Mater.* **2016**, *28*, 10588.
[2] A. Mobasseri, A. Faroni, B. M. Minogue, S. Downes, G. Terenghi, A. J. Reid, *Tissue Eng., Part A* **2015**, *21*, 1152.
[3] S. Nesbitt, W. Scott, J. Macione, S. Kotha, *Materials* **2015**, *8*, 1841.
[4] S. H. Wu, B. Duan, P. H. Liu, C. D. Zhang, X. H. Qin, J. T. Butcher, *ACS Appl. Mater. Interfaces* **2016**, *8*, 16950.
[5] Z. F. Lin, X. J. Zhao, S. Chen, C. Du, *J. Mater. Chem. B* **2017**, *5*, 1015.
[6] S. Ostrovidov, M. Ebrahimi, H. Bae, H. K. Nguyen, S. Salehi, S. B. Kim, A. Kumatani, T. Matsue, X. T. Shi, K. Nakajima, S. Hidema, M. Osanai, A. Khademhosseini, *ACS Appl. Mater. Interfaces* **2017**, *9*, 42444.
[7] J. Zhang, X. Y. Ma, D. Lin, H. S. Shi, Y. Yuan, W. Tang, H. J. Zhou, H. Guo, J. C. Qian, C. S. Liu, *Biomaterials* **2015**, *53*, 251.
[8] K. Minami, Y. Kasuya, T. Yamazaki, Q. M. Ji, W. Nakanishi, J. P. Hill, H. Sakai, K. Ariga, *Adv. Mater.* **2015**, *27*, 4020.
[9] T. L. Downing, J. Soto, C. Morez, T. Houssin, A. Fritz, F. L. Yuan, J. L. Chu, S. Patel, D. V. Schaffer, S. Li, *Nat. Mater.* **2013**, *12*, 1154.
[10] P. Zorlutuna, N. Annabi, G. Camci-Unal, M. Nikkhah, J. M. Cha, J. W. Nichol, A. Manbachi, H. Bae, S. C. Chen, A. Khademhosseini, *Adv. Mater.* **2012**, *24*, 1782.
[11] X. J. Zan, S. Feng, E. Balizan, Y. Lin, Q. Wang, *ACS Nano* **2013**, *7*, 8385.
[12] C. A. Poland, R. Duffin, I. Kinloch, A. Maynard, W. A. Wallace, A. Seaton, V. Stone, S. Brown, W. MacNee, K. Donaldson, *Nat. Nanotechnol.* **2008**, *3*, 423.

[13] M. X. Liu, Z. X. Jia, D. M. Jia, C. R. Zhou, *Prog. Polym. Sci.* **2014**, *39*, 1498.
[14] Y. Lvov, W. C. Wang, L. Q. Zhang, R. Fakhrullin, *Adv. Mater.* **2016**, *28*, 1227.
[15] Y. M. Lvov, D. G. Shchukin, H. Mohwald, R. R. Price, *ACS Nano* **2008**, *2*, 814.
[16] R. R. Price, B. P. Gaber, Y. M. Lvov, *J. Microencapsulation* **2001**, *18*, 713.
[17] Z. R. Long, Y. P. Wu, H. Y. Gao, J. Zhang, X. Ou, R. R. He, M. X. Liu, *J. Mater. Chem. B* **2018**, *6*, 7204.
[18] J. Rexer, E. Anderson, *Polym. Eng. Sci.* **1979**, *19*, 1.
[19] M. X. Liu, Z. H. Huo, T. F. Liu, Y. Shen, R. He, C. R. Zhou, *Langmuir* **2017**, *33*, 3088.
[20] B. J. Ma, S. Zhang, F. Liu, J. Z. Duan, S. C. Wang, J. Han, Y. H. Sang, X. Q. Yu, D. Li, W. Tang, *ACS Appl. Mater. Interfaces* **2017**, *9*, 33717.
[21] A. Skogberg, A.-J. Maki, M. Mettanen, P. Lahtinen, P. Kallio, *Biomacromolecules* **2017**, *18*, 3936.
[22] P. Gupta, S. Sharan, P. Roy, D. Lahiri, *Carbon* **2015**, *95*, 715.
[23] C. Y. Du, M. Li, M. Cao, S. C. Feng, H. Guo, B. A. Li, *Carbon* **2018**, *126*, 197.
[24] Y. J. Cha, D. K. Yoon, *Adv. Mater.* **2017**, *29*, 1604247.
[25] E. Joussein, S. Petit, J. Churchman, B. Theng, D. Righi, B. Delvaux, *Clay Miner.* **2005**, *40*, 383.
[26] B. Szczepanik, P. Słomkiewicz, M. Garnuszek, K. Czech, D. Banaś, A. Kubala-Kukuś, I. Stabrawa, *J. Mol. Struct.* **2015**, *1084*, 16.
[27] S. Q. Deng, J. N. Zhang, L. Ye, J. S. Wu, *Polymer* **2008**, *49*, 5119.
[28] G. W. Brindley, Robinson, K., Macewan, D. M. C, *Nature* **1946**, *157*, 225.
[29] P. Sun, G. M. Liu, D. Lv, X. Dong, J. S. Wu, D. J. Wang, *RSC Adv.* **2015**, *5*, 52916.
[30] Y. F. Zhao, G. Cavallaro, Y. Lvov, *J. Colloid Interface Sci.* **2015**, *440*, 68.
[31] G. Lazzara, G. Cavallaro, A. Panchal, R. Fakhrullin, A. Stavitskaya, V. Vinokurov, Y. Lvov, *Curr. Opin. Colloid Interface Sci.* **2018**, *35*, 42.
[32] G. Cavallaro, G. Lazzara, S. Milioto, G. Palmisano, F. Parisi, *J. Colloid Interface Sci.* **2014**, *417*, 66.
[33] R. He, M. X. Liu, Y. Shen, R. Liang, W. Liu, C. R. Zhou, *Mater. Sci. Eng., C* **2018**, *85*, 170.
[34] A. D. Hughes, J. Mattison, L. T. Western, J. D. Powderly, B. T. Greene, M. R. King, *Clin. Chem.* **2012**, *58*, 846.
[35] B. Wang, A. L. Weldon, P. Kumnorkaew, B. Xu, J. F. Gilchrist, X. H. Cheng, *Langmuir* **2011**, *27*, 11229.
[36] E. Ye, X. J. Loh, *Aust. J. Chem.* **2013**, *66*, 997.
[37] P. Clark, P. Connolly, A. Curtis, J. Dow, C. Wilkinson, *J. Cell Sci.* **1991**, *99*, 73.
[38] F. Johansson, M. Jonsson, K. Alm, M. Kanje, *Exp. Cell Res.* **2010**, *316*, 688.
[39] P. Weiss, H. B. Hiscoe, *J. Exp. Zool.* **1948**, *107*, 315.
[40] J. A. Kim, E. Y. Jang, T. J. Kang, S. Yoon, R. Ovalle-Robles, W. J. Rhee, T. Kim, R. H. Baughman, Y. H. Kim, T. H. Park, *Integr. Biol.* **2012**, *4*, 587.
[41] Y. J. Yang, X. L. Wang, T. C. Huang, X. H. Hu, N. Kawazoe, W. B. Tsai, Y. N. Yang, G. P. Chen, *J. Mater. Chem. B* **2018**, *6*, 5424.
[42] D. Zhang, M. B. Sun, J. M. Lee, A. A. Abdeen, K. A. Kilian, *J. Biomed. Mater. Res., Part A* **2016**, *104*, 1212.
[43] G. A. Chen, T. G. Gharib, C. C. Huang, J. G. Taylor, D. E. Misek, S. R. Kardia, T. J. Giordano, M. D. Iannettoni, M. B. Orringer, S. M. Hanash, D. G. Beer, *Mol. Cell. Proteomics* **2002**, *1*, 304.
[44] T. J. Griffin, S. P. Gygi, T. Ideker, B. Rist, J. Eng, L. Hood, R. Aebersold, *Mol. Cell. Proteomics* **2002**, *1*, 323.
[45] J. P. Fu, Y.-K. Wang, M. T. Yang, R. A. Desai, X. Yu, Z. J. Liu, C. S. Chen, *Nat. Methods* **2010**, *7*, 733.
[46] S.-T. Wu, U. Efron, L. D. Hess, *Appl. Opt.* **1984**, *23*, 3911.
[47] R. He, M. X. Liu, Y. Shen, Z. R. Long, C. R. Zhou, *J. Mater. Chem. B* **2017**, *5*, 1712.
[48] X. J. Zhao, S. Chen, Z. F. Lin, C. Du, *Carbohydr. Polym.* **2016**, *148*, 98.
[49] X. J. Zhao, L. Y. Zhou, Q. T. Li, Q. X. Zou, C. Du, *Carbohydr. Polym.* **2018**, *195*, 225.
[50] L.-F. Tseng, P. T. Mather, J. H. Henderson, *Acta Biomater.* **2013**, *9*, 8790.
[51] C. Ayres, G. L. Bowlin, S. C. Henderson, L. Taylor, J. Shultz, J. Alexander, T. A. Telemeco, D. G. Simpson, *Biomaterials* **2006**, *27*, 5524.
[52] C. Williams, A. W. Xie, M. Yamato, T. Okano, J. Y. Wong, *Biomaterials* **2011**, *32*, 5625.